



HAL
open science

Mercury Isotopes in Deep-Sea Epibenthic Biota Suggest Limited Hg Transfer from Photosynthetic to Chemosynthetic Food Webs

Jingjing Yuan, Yi Liu, Shun Chen, Xiaotong Peng, Yu-Feng Li, Songjing Li, Rui Zhang, Wang Zheng, Jiubin Chen, Ruoyu Sun, et al.

► **To cite this version:**

Jingjing Yuan, Yi Liu, Shun Chen, Xiaotong Peng, Yu-Feng Li, et al.. Mercury Isotopes in Deep-Sea Epibenthic Biota Suggest Limited Hg Transfer from Photosynthetic to Chemosynthetic Food Webs. Environmental Science and Technology, inPress, 10.1021/acs.est.3c01276 . hal-04068003

HAL Id: hal-04068003

<https://hal.science/hal-04068003>

Submitted on 13 Apr 2023

HAL is a multi-disciplinary open access archive for the deposit and dissemination of scientific research documents, whether they are published or not. The documents may come from teaching and research institutions in France or abroad, or from public or private research centers.

L'archive ouverte pluridisciplinaire **HAL**, est destinée au dépôt et à la diffusion de documents scientifiques de niveau recherche, publiés ou non, émanant des établissements d'enseignement et de recherche français ou étrangers, des laboratoires publics ou privés.

Mercury Isotopes in Deep-Sea Epibenthic Biota Suggest Limited Hg Transfer from Photosynthetic to Chemosynthetic Food Webs

Jingjing Yuan¹, Yi Liu¹, Shun Chen², Xiaotong Peng², Yu-Feng Li³, Songjing Li¹, Rui Zhang¹, Wang Zheng¹, Jiubin Chen¹, Ruoyu Sun^{1*}, Lars-Eric Heimbürger-Boavida⁴

¹Institute of Surface-Earth System Science, School of Earth System Science, Tianjin University, 300072 Tianjin, China.

²Deep Sea Science Division, Institute of Deep Sea Science and Engineering, Chinese Academy of Sciences, 572000 Sanya, Hainan, China.

³CAS-HKU Joint Laboratory of Metallomics on Health and Environment, CAS Key Laboratory for Biomedical Effects of Nanomaterials and Nanosafety, Beijing Metallomics Facility, Institute of High Energy Physics, Chinese Academy of Sciences, 100049 Beijing, China.

⁴Aix Marseille Université, CNRS/INSU, Université de Toulon, IRD, Mediterranean Institute of Oceanography (MIO) UM 110, 13288 Marseille, France.

Corresponding Author

*Ruoyu Sun (ruoyu.sun@tju.edu.cn).

19 **ABSTRACT**

20 Deep oceans receive mercury (Hg) from upper oceans, sediment diagenesis, and submarine volcanism;
21 meanwhile, sinking particles shuttle Hg to marine sediments. Recent studies showed that Hg in the trench
22 fauna mostly originated from monomethylmercury (MMHg) of the upper marine photosynthetic food webs.
23 Yet, Hg sources in the deep-sea chemosynthetic food webs are still uncertain. Here, we report Hg
24 concentrations and stable isotopic compositions of indigenous biota living at hydrothermal fields of the
25 Indian Ocean Ridge and a cold seep of the South China Sea along with hydrothermal sulfide deposits. We
26 find that Hg is highly enriched in hydrothermal sulfides, which correlated with varying Hg concentrations in
27 inhabited biota. Both the hydrothermal and cold seep biota have small fractions (<10%) of Hg as MMHg
28 and slightly positive $\Delta^{199}\text{Hg}$ values. These $\Delta^{199}\text{Hg}$ values are slightly higher than those in near-field sulfides
29 but are 1 order of magnitude lower than the trench counterparts. We suggest that deep-sea chemosynthetic
30 food webs mainly assimilate Hg from ambient seawater/sediments and hydrothermal fluids formed by
31 percolated seawater through magmatic/mantle rocks. The MMHg transfer from photosynthetic to
32 chemosynthetic food webs is likely limited. The contrasting Hg sources between chemosynthetic and trench
33 food webs highlight Hg isotopes as promising tools to trace the deep-sea Hg biogeochemical cycle.

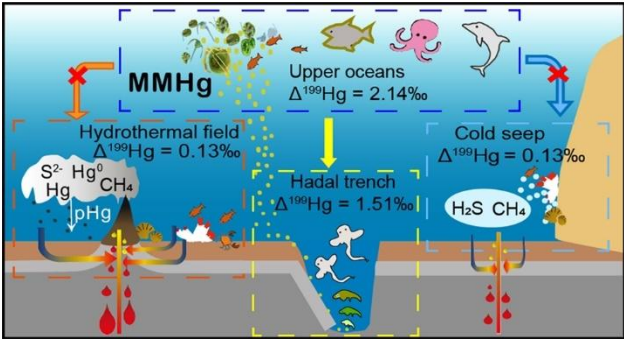
34 **KEYWORDS**

35 marine mercury cycling, oceans, hydrothermal fluids, cold seeps, biota, mercury isotopes

36 **SYNOPSIS**

37 Mercury isotope measurement is a promising tool to track the food sources and Hg biogeochemical cycle in
38 deep-sea chemosynthetic ecosystems.

40 **Table of Content (TOC)/Abstract Art**



41

42

43 1. Introduction

44 Mercury (Hg) is released into Earth's surface environment from natural and anthropogenic sources ¹.
45 One of the most toxic forms of Hg is monomethylmercury (MMHg), which bioaccumulates and
46 biomagnifies in marine food webs. In the open oceans, MMHg is thought to be mostly derived from *in situ*
47 production within the upper marine (<1000 m) waters ^{2,3}. However, it is still uncertain if MMHg could be *in*
48 *situ* produced in deep marine (>1000 m) waters and sediments. Deep oceans receive Hg from upper oceans
49 via particle settling ^{4, 5}, deep water formation ⁶ and occasionally carrion (e.g., whalefall) ⁷. Thus,
50 anthropogenic Hg can be brought into deep oceans and finally buried into sediments. Meanwhile, the
51 sinking particles and seafloor sediments could also release Hg during remineralization and diagenesis
52 processes ^{4, 5, 8, 9}. In addition, geogenic Hg could be discharged into the deep oceans via submarine
53 hydrothermal vents mostly surrounding mid-ocean ridges, back-arc basins, and submarine volcanic arcs, and
54 possibly cold seeps located at continental slopes near the tectonic plate boundaries ¹⁰⁻¹⁵.

55 To date, the submarine geogenic Hg is poorly constrained but is potentially important at volcanic- and
56 hydrothermal-active areas. An upper range value of 600 Mg yr⁻¹ for the submarine hydrothermal Hg flux has
57 been estimated in the UNEP report ^{1, 16, 17}, although it may vary orders of magnitude (20-2000 Mg yr⁻¹)
58 based on several field measurements of hydrothermal fluids ¹⁰. For example, Lamborg, et al. (2006) ¹² found
59 slightly enhanced levels of total Hg (THg) nearly all present as MMHg in fluids (~10 pM) compared to
60 seawater (~1-2 pM) from the Sea Cliff submarine hydrothermal field, Gorda Ridge. Assuming the
61 hydrothermal Hg flux from this site was representative of global submarine hydrothermal systems, they
62 estimated a global hydrothermal Hg flux of 20 to 80 Mg yr⁻¹. In contrast, Crepo-Medina, et al. ¹⁸ showed
63 that the fluid MMHg in East Pacific Rise deep-sea vents was a minor species (<12.5%) with concentrations
64 mostly below the detection limits of <1.5 pM, but THg concentrations were extremely high in both diffuse
65 (12 to 450 pM) and focused flow vents (3500 to 11000 pM). The authors suggested that hydrothermal fluids

66 may contribute $\sim 2000 \text{ Mg yr}^{-1}$ of Hg to the ocean. Besides, one hydrothermal fluid sample in the Guaymas
67 Basin, Gulf of California was reported to have as high as 11000 pM of THg¹⁹, and two hydrothermal fluid
68 samples at Tonga back-arc had low THg concentrations of 5 and 10 pM ¹¹. As for cold seeps, there is no
69 estimation of the Hg flux. Therefore, we currently could not thoroughly evaluate hydrothermal and cold seep
70 Hg inputs to the ocean, and integrate them into marine Hg models. In addition, it is still largely unknown
71 how submarine geogenic Hg affects deep marine Hg biogeochemical cycling.

72 Mercury has seven stable isotopes, and the ratios of these isotopes have been developed as diagnostic
73 tracers to understand biogeochemical cycles of Hg in Earth's ecosystems^{20, 21}. Hg isotopes exhibit
74 significant mass-dependent fractionation (MDF, represented by $\delta^{202}\text{Hg}$) in nearly all biogeochemical Hg
75 transformations, and large mass-independent fractionation of odd-mass number isotopes (odd-MIF,
76 represented by $\Delta^{199}\text{Hg}$ and $\Delta^{201}\text{Hg}$) mainly in photochemical Hg transformations, notably photoreduction of
77 inorganic Hg(II) and photodegradation of MMHg²²⁻²⁵. Much smaller magnitude but significant even-mass
78 number MIF (even-MIF, represented by $\Delta^{200}\text{Hg}$ and $\Delta^{204}\text{Hg}$) has also been observed primarily in
79 atmospheric precipitation, which is hypothesized to be linked to photochemistry of gaseous Hg in the upper
80 atmosphere²⁶⁻²⁹. Numerous studies have used Hg isotopic signatures, especially MIF, in aquatic food webs
81 to trace *in vitro* Hg sources and transformation in aqueous systems, because *in vivo* metabolic processes and
82 the accumulation and trophic transfer of Hg within food webs cause insignificant MIF³⁰⁻³³. As proxied by
83 marine pelagic fishes, $\Delta^{199}\text{Hg}$ values of MMHg in upper oceans decrease systematically with depth, which is
84 primarily caused by great photo-degradation of bioavailable MMHg in the surface ocean followed by the
85 transport of surface MMHg via sinking particles and mixing with subsurface MMHg³⁴⁻³⁷.

86 There is still relatively little Hg isotope research in the deep ocean, even though it accounts for over 70%
87 of the whole ocean's volume. Recent studies on Hg isotopic compositions in hadal fauna and sediments from
88 the deepest ocean (i.e., trenches, $>6000 \text{ m}$) indicated that the biotic Hg was mostly derived of MMHg from

89 the upper oceans, including Hg from anthropogenic sources³⁸⁻⁴⁰. In addition to trenches, hydrothermal vents
90 and cold seeps also host high densities of endemic fauna, yet their Hg sources remain to be controversial^{12,}
91 ¹⁴. The food and energy sources of hydrothermal and cold seep ecosystems rely mainly on chemosynthetic
92 bacteria and archaea at the bottom of food webs^{41,42}. They are quite different from trench ecosystems that
93 mainly rely on sinking organic matter photosynthesized at the upper oceans⁴³⁻⁴⁵. Moreover, hydrothermal
94 vents and cold seeps could potentially release large amounts of geogenic Hg which might disperse into the
95 deep oceans and then is accumulated in the surrounding ecosystems^{11,46}.

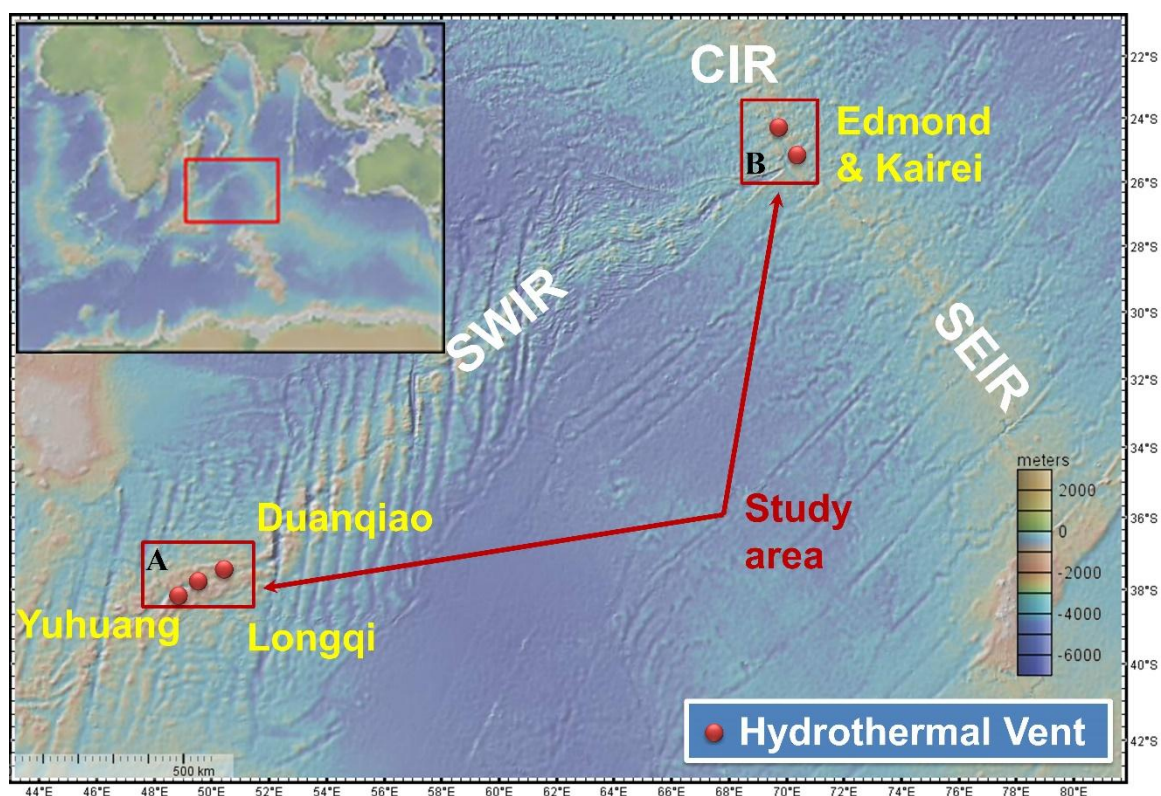
96 In this study, we report Hg isotopic compositions of submarine hydrothermal sulfides and indigenous
97 epibenthic biota living at several different hydrothermal vent fields from the Indian Ocean Ridge and a cold
98 seep from the South China Sea. Combining THg/MMHg concentrations, bulk carbon/nitrogen stable
99 isotopes of biota, we aim to trace the sources of Hg of chemosynthetic food webs and to understand how
100 submarine geogenic Hg affects the Hg biogeochemical cycling in deep-sea extreme ecosystems.

101 **2. Materials and Methods**

102 **2.1. Sample Collection and Pretreatment**

103 During the Chinese cruise TS10 from November 10th, 2018 to March 10th, 2019, video survey and
104 sampling were undertaken using the submersible “Shenhai Yongshi” (Deep-Sea Warrior) that was equipped
105 with a seven-function manipulator at the Indian Ocean Ridge. We selected 14 surface layer bulk sulfides
106 (Table S1) and ~30 biota samples (Table S2; all invertebrates, e.g., *Bathymodiolus* mussels, *Alviniconcha*
107 snails, *Peltospiridae* gastropods, *Galatheidae* crabs and *Rimicaris* shrimps) from four deep hydrothermal
108 fields (HFs), with two (Longqi HF and Duanqiao HF) from the Southwest Indian Ridge (SWIR) of
109 ultra-slow spreading rates (7 to 16 mm yr⁻¹) and two (Edmond HF and Kairei HF) from the Central Indian
110 Ridge (CIR) of intermediate spreading rates (50 to 60 mm yr⁻¹) (Figure 1 and Supporting Information). The

111 spreading rate is defined as the relative separation rate of the plates on either side of the mid-ocean ridge⁴⁷.
112 In addition, the ROV (Remotely Operated Vehicle) of ROPOS (Remotely Operated Platform for Ocean
113 Science) onboard R/V Tan Kah Kee was used during Dive 2046 to sample epifauna at the Site F cold seep of
114 the South China Sea in April 2018, from which *Gigantidas platifrons* and *Bathymodiolus aduloides* mussels
115 were selected in our study^{48, 49}.



116

117 **Figure 1.** Geological map of Indian Ocean Ridge. The studied Longqi and Duanqiao hydrothermal fields in
118 SWIR and Edmond and Kairei hydrothermal fields in CIR are shown in red boxes. Note: SWIR, Southwest
119 Indian Ridge; CIR, Central Indian Ridge; SEIR, Southeast Indian Ridge.

120

121

122

123

124

125

126

The captured biota samples were immediately frozen at -80 °C upon loading on deck. After returning to the laboratory, they were carefully washed with 18.2 MΩ cm Milli-Q water, and then their muscle and gill were separated using pre-cleaned surgical scissors and tweezers. For nearly all the biota samples, measurements were performed only on their muscle tissues due to the limited mass of gill. Only one hydrothermal biota sample (SY138-mussel) was measured on gill rather than muscle. Two cold seep mussels were measured on both gill and muscle. Individuals of similar size and from the same location were typically combined to one sample to increase the sampling representativeness and Hg mass required for

127 isotope analysis. Before measurement of Hg concentrations and isotopic compositions, all the samples were
128 freeze-dried and homogenized.

129 **2.2. THg, MMHg Concentrations and Hg Isotope Measurement**

130 THg concentrations of all sulfide and biota samples (Tables S1, S2) were quantified by cold vapor
131 atomic absorption spectrometry (CV-AAS, DMA-80 evo Direct Mercury Analyzer) following the US-EPA
132 method 7473⁵⁰. Detectable MMHg concentrations in the biota samples (Table S2) were determined by cold
133 vapor gas chromatography atomic fluorescence spectrometry (CV-GC-AFS, Tekran 2700) following the
134 US-EPA method 1630⁵¹ after solvent extraction using KOH/CH₃OH solution, and ethylation by NaBEt₄ in
135 closed purge vessels⁵². Before Hg isotope measurement, the sulfides and biota were digested separately by
136 HNO₃, HCl and BrCl, and HNO₃, H₂O₂ and BrCl at ~100°C for 48 h⁵³, followed by Hg purification using
137 the anion-exchange chromatographic method^{53, 54}. Procedural blanks and certified reference materials
138 (CRMs, DORM-4 and TORT-3 for biota; MESS-4, NIST SRM-2702, and NIST SRM-1944 for sulfides)
139 were processed with the samples in the same manner. THg concentrations in all purified solutions were
140 determined by the cold vapor atomic fluorescence spectrometry (CV-AFS, Tekran 2600) according to
141 US-EPA method 1631E⁵⁵. The procedural blanks accounted for <1% of Hg mass in the samples, and the Hg
142 recoveries were in the range of 93-103% for procedural CRMs and 84-108% for samples. All the purified
143 sample and CRM solutions were diluted with ultrapure water to Hg concentrations of 0.5-1 ng g⁻¹ and were
144 measured for Hg isotope ratios by coupling a customized cold vapor generation system to multi-collector
145 inductively coupled plasma mass spectrometry (MC-ICPMS, Nu Plasma 3D at Tianjin University, China).
146 Mass bias of MC-ICP-MS was corrected by an internal NIST SRM-997 Tl standard using the exponential
147 law and by the primary NIST SRM-3133 Hg standard using the standard sample bracketing method. Details
148 on the analytical procedures for concentrations of THg and MMHg, and Hg isotope ratios are provided in
149 the Supporting Information.

150 The Hg isotope ratio is expressed as $\delta^{xxx}\text{Hg}$ (‰, xxx = 199, 200, 201, 202, 204) by normalizing to the
151 primary NIST SRM-3133 Hg standard:

$$152 \quad \delta^{xxx}\text{Hg}(\text{‰}) = \left(\frac{({}^{xxx}\text{Hg}/{}^{198}\text{Hg})_{\text{sample}}}{({}^{xxx}\text{Hg}/{}^{198}\text{Hg})_{\text{NIST SRM-3133}}} - 1 \right) \times 1000 \quad (1)$$

153 MIF value is denoted as $\Delta^{xxx}\text{Hg}$ (‰, xxx = 199, 200, 201, 204), representing the difference between the
154 measured $\delta^{xxx}\text{Hg}$ value and that predicted from $\delta^{202}\text{Hg}$ using a kinetic MDF law ⁵⁶:

$$155 \quad \Delta^{xxx}\text{Hg}(\text{‰}) = \delta^{xxx}\text{Hg} - \beta^{xxx} \times \delta^{202}\text{Hg} \quad (2)$$

156 The mass-dependent scaling factor β^{xxx} is 0.2520 for ¹⁹⁹Hg, 0.5024 for ²⁰⁰Hg, 0.7520 for ²⁰¹Hg, and
157 1.4930 for ²⁰⁴Hg.

158 The Hg isotope ratios of the secondary standard NIST SRM-8610 and procedural CRMs analyzed
159 during different analytic sessions agreed with those reported in previous studies (Table S3) ^{52, 56-59}. The
160 typical 2σ analytic uncertainties of samples were estimated as the larger 2SD uncertainties of Hg isotope
161 ratios between NIST SRM-8610 and procedural CRMs (DORM-4 and TORT-3 for biota; MESS-4, NIST
162 SRM-2702 and NIST SRM-1944 for sulfides). The 2SE uncertainties of Hg isotope ratios in samples with
163 replicate analyses were applied as the analytic uncertainties only when they were larger than the typical 2σ
164 analytic uncertainties ⁵⁶.

165 **2.3. Stable Carbon and Nitrogen Isotope Analysis**

166 Carbon and nitrogen isotope ratios were determined by gas stable isotope ratio mass spectrometer (253
167 Plus, Thermo Fisher Scientific) equipped with a Flash 2000 HT elemental analyzer. The carbon and nitrogen
168 isotope ratios are expressed as δ (‰) notations by referring to their respective standards (Vienna Pee Dee
169 Belemnite, V-PDB and atmospheric N₂):

$$170 \quad \delta^{13}\text{C}(\text{‰}) = \left(\frac{({}^{13}\text{C}/{}^{12}\text{C})_{\text{sample}}}{({}^{13}\text{C}/{}^{12}\text{C})_{\text{V-PDB}}} - 1 \right) \times 1000 \quad (3)$$

$$171 \quad \delta^{15}\text{N}(\text{‰}) = \left(\frac{({}^{15}\text{N}/{}^{14}\text{N})_{\text{sample}}}{({}^{15}\text{N}/{}^{14}\text{N})_{\text{N}_2}} - 1 \right) \times 1000 \quad (4)$$

172 The typical analytic uncertainty assessed by the internal standards (IAEA-600, USGS-40 and USGS-41)
173 were within 0.2‰ for $\delta^{13}\text{C}$ and within 0.3‰ for $\delta^{15}\text{N}$.

174 **2.4. Data Analysis**

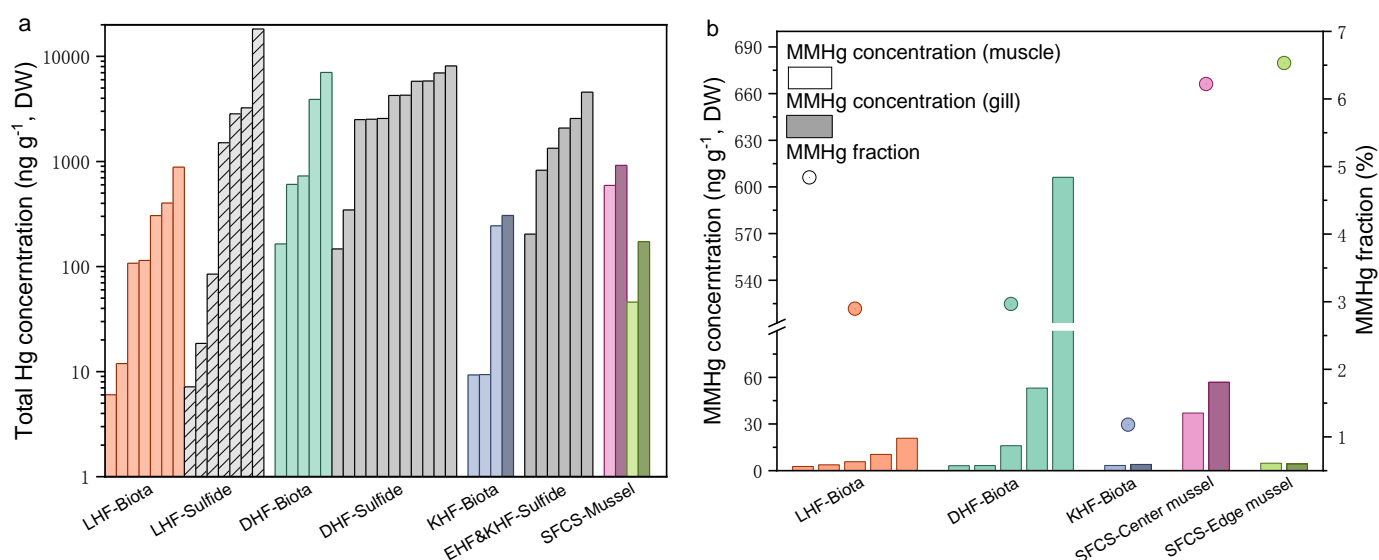
175 The correlations between studied variables were calculated using the linear regression correlation
176 analysis of the software OriginPro 2021. The fitting curves are bounded by 95% confidence bands, with
177 Pearson's R-Square and P-values calculated by algorithms of the software. Two-side analysis of variance
178 (ANOVA) was used to assess if the regression slope is significantly different from zero at $\alpha = 0.05$. The
179 isotope mixing model was run using a Monte Carlo simulation approach ($n = 10,000$ times) through the
180 pseudorandom number generation function of the MatLab software (R2016b, MathWorks)³⁸. Data were
181 checked for normality (Shapiro-Wilks tests) and variance homogeneity (Bartlett's tests). Parametric and
182 non-Parametric statistic methods of the software SPSS 19.0 is used compare the same variable (e.g., THg
183 and MMHg concentrations and isotope data) between two different groups.

184 **3. Results and Discussion**

185 **3.1. Hydrothermal Sulfides as Important Hg Sinks**

186 THg concentrations in studied massive sulfides range over three orders of magnitude from 7 to $1.8 \times$
187 10^4 ng g^{-1} (dry weight), with an average of $2690 \pm 4689 \text{ ng g}^{-1}$ (mean \pm 1SD, $n = 14$) (Table S1, Figure 2).
188 These high and large scatter of Hg concentrations are consistent with the previously reported values in
189 massive and chimney sulfides and sulfide minerals of Duanqiao and Yuhuang HF's from SWIR (350 to $4.4 \times$
190 10^4 ng g^{-1}) and hydrothermally-altered sediments in CIR (17 to $1.3 \times 10^4 \text{ ng g}^{-1}$)^{15, 60}, corroborating the
191 viewpoint that Hg discharged from hydrothermal vent fluids is preferably removed by co-precipitated
192 sulfides^{60, 61}. The Hg MDF and odd-MIF values ($\delta^{202}\text{Hg}$: -1.17 to -0.34‰, $-0.77 \pm 0.25\%$; $\Delta^{199}\text{Hg}$: -0.06 to
193 0.16‰, $0.05 \pm 0.06\%$; $n = 14$) (Table S1, Figure 3) of our massive sulfides are also comparable ($P > 0.05$) to

194 those of previously reported SWIR sulfides ($\delta^{202}\text{Hg}$: -1.23 to -0.05‰, $-0.59 \pm 0.30\%$; $\Delta^{199}\text{Hg}$: -0.10 to
 195 0.20‰, $0.05 \pm 0.06\%$; $n = 42$)¹⁵. The even-MIF values ($\Delta^{200}\text{Hg} = 0.01 \pm 0.01\%$, -0.01 to 0.03‰; $\Delta^{204}\text{Hg} =$
 196 $0.00 \pm 0.03\%$, -0.07 to 0.08‰) of our massive sulfides are mostly within their analytic uncertainty (Figure
 197 S1). In Table 1, we summarize the statistic values on Hg isotope compositions of sulfides in different
 198 hydrothermal fields from Indian Ocean Ridge: Longqi ($\delta^{202}\text{Hg} = -0.77 \pm 0.22\%$; $\Delta^{199}\text{Hg} = 0.06 \pm 0.06\%$; n
 199 $= 7$), Duanqiao ($\delta^{202}\text{Hg} = -0.35 \pm 0.18\%$; $\Delta^{199}\text{Hg} = 0.05 \pm 0.03\%$; $n = 11$) and Yuhuang ($\delta^{202}\text{Hg} = -0.68 \pm$
 200 0.29% ; $\Delta^{199}\text{Hg} = 0.05 \pm 0.07\%$; $n = 32$) from SWIR and Edmond and Kairei ($\delta^{202}\text{Hg} = -0.78 \pm 0.33\%$;
 201 $\Delta^{199}\text{Hg} = 0.03 \pm 0.07\%$; $n = 6$) from CIR. In comparison, they are quite similar to Hg isotopic compositions
 202 of Earth's silicate crust ($\delta^{202}\text{Hg} = -0.78 \pm 0.51\%$; $\Delta^{199}\text{Hg} = 0.00 \pm 0.08\%$) summarized in Sun, et al.⁶², bulk
 203 Hg emissions from passively degassing volcanoes ($\delta^{202}\text{Hg} = -0.76 \pm 0.11\%$; $\Delta^{199}\text{Hg} = 0.05 \pm 0.03\%$; $n = 9$)
 204 ^{62, 63}, and chimney pieces and fluid precipitate from the Guaymas Basin sea-floor rift ($\delta^{202}\text{Hg} = -0.23 \pm$
 205 0.19% ; $\Delta^{199}\text{Hg} = 0.02 \pm 0.02\%$; $n = 3$)¹⁹. However, based on ³He-rich lavas from Samoa and Iceland,
 206 primordial mantle ($\delta^{202}\text{Hg} = -1.72 \pm 1.15\%$; $\Delta^{199}\text{Hg} = 0.00 \pm 0.10\%$; $n = 11$) appears to have significantly
 207 lower $\delta^{202}\text{Hg}$ values⁶⁴.

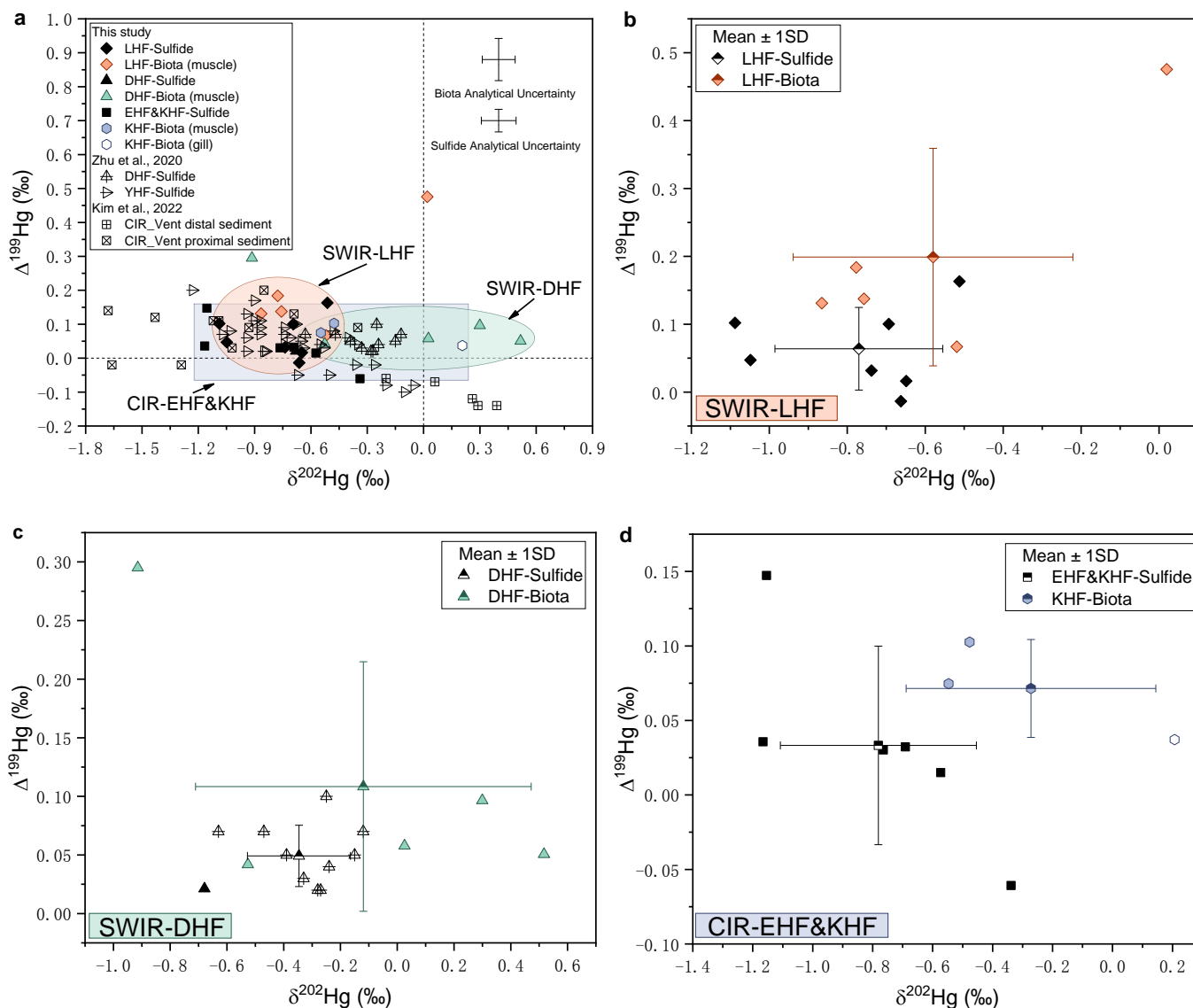


208

209 **Figure 2.** Plots showing THg (a), and MMHg concentrations and MMHg fractions (b). THg concentrations
 210 (logarithmic scale; DW: dry weight) in sulfides and biota from different hydrothermal fields at the Indian
 211 Ocean Ridge and mussels from the Site F cold seep (SFCS) at the South China Sea (a); Detectable MMHg
 212 concentrations and site-specific means of MMHg fractions in biota (b). Note: LHF: Lonqi HF; DHF:

213 Duanqiao HF; KHF: Kairei HF; EHF: Edmond HF; SFCS-Center mussel: mussel near the center of the Site
 214 F cold seep; SFCS-Edge mussel: mussel at the edge of the Site F cold seep.

215



216

217

218 **Figure 3.** $\Delta^{199}\text{Hg}$ versus $\delta^{202}\text{Hg}$ in hydrothermal sulfides and biota from the Indian Ocean Ridge (a) and
 219 individual hydrothermal fields including Longqi HF (LHF) (b) and Duanqiao HF (DHF) (c) at the Southwest
 220 Indian Ridge (SWIR), and Kairei HF (KHF) and Edmond HF (EHF) (d) at the Central Indian Ridge (CIR).
 221 The ellipses and rectangle in subplot (a) are used to outline the variation ranges of Hg isotopic compositions
 222 of individual hydrothermal fields. The error bars in subplots b-d denote mean $\pm 1\text{SD}$

223

224
225**Table 1.** Summary of THg Concentrations and Isotopic Compositions of Sulfides, Biota, and Vent-Proximal Sediments from Different Hydrothermal Fields in the Indian Ocean Ridge.

Hydrothermal fields	type	n	Hg concentration (ng g ⁻¹)					$\delta^{202}\text{Hg}$ (‰)					$\Delta^{199}\text{Hg}$ (‰)					$\Delta^{201}\text{Hg}$ (‰)				
			mean	1SD	min	median	max	mean	1SD	min	median	max	mean	1SD	min	median	max	mean	1SD	min	median	max
Longqi HF,	sulfide	7	3702	6542	7.2	1510	18217	-0.77	0.22	-1.09	-0.69	-0.51	0.06	0.06	-0.01	0.05	0.16	0.04	0.04	-0.01	0.03	0.11
SWIR	biota	7	261	311	6.0	114	882	-0.58	0.36	-0.87	-0.76	0.02	0.20	0.16	0.07	0.14	0.48	0.15	0.11	0.07	0.11	0.33
Duanqiao HF,	sulfide*	11	3937	2590	147	4248	8121	-0.35	0.18	-0.68	-0.28	-0.12	0.05	0.03	0.02	0.05	0.10	0.04	0.02	0.01	0.03	0.07
SWIR	biota	5	2488	2950	164	728	7045	-0.12	0.59	-0.91	0.03	0.52	0.11	0.11	0.04	0.06	0.30	0.07	0.10	-0.01	0.04	0.24
Yuhuang HF,	sulfide*	32	5306	7722	435	2686	44035	-0.68	0.29	-1.23	-0.73	-0.05	0.05	0.07	-0.10	0.06	0.20	0.03	0.06	-0.10	0.03	0.19
SWIR																						
Edmond & Kairei HFs,	sulfide	6	1932	1548	203	1709	4574	-0.78	0.33	-1.17	-0.73	-0.34	0.03	0.07	-0.06	0.03	0.15	0.01	0.03	-0.03	0.01	0.06
CIR																						
Kairei HF,	biota	4	142	156	9	127	307	-0.27	0.42	-0.55	-0.48	0.21	0.07	0.03	0.04	0.07	0.10	0.05	0.01	0.04	0.05	0.06
CIR																						
CIR	vent-proximal sediment**	5	6857	4811	1042	5329	12944	0.16	0.23	-0.20	0.26	0.39	-0.11	0.04	-0.14	-0.12	-0.06	-0.08	0.01	-0.10	-0.08	-0.06

226
227

*Most of sulfides from Duanqiao HF (n = 10) and all sulfides from Yuhuang HF are from Zhu, et al. (2020)¹⁵; **hydrothermal-altered sediments are cited from Kim, et al. (2022)⁶⁰; n: number of the combined samples.

228

229 During the formation of submarine hydrothermal fluids, the conductively heated seawater leaches,
230 concentrates and transports Hg from magmatic/mantle rocks. Previous studies showed that these
231 hydrothermal processes including boiling of hydrothermal fluids, aqueous Hg⁰ separation, and redox
232 reactions could cause significant MDF.^{19, 65, 66} Similarly, the deposition of the sulfides from hydrothermal
233 fluids was also suggested to induce significant MDF, enriching sulfides with light Hg isotopes.^{15, 65-67}
234 However, significant MIF unlikely occurs in these processes. In general, the ranges of $\delta^{202}\text{Hg}$ in sulfides
235 from Indian Ocean Ridge (-1.23 to -0.05‰ for SWIR and -1.17 to -0.34‰ for CIR, Table 1) are >5 times
236 smaller than those documented for subaerial hydrothermal systems (-3.69 to 2.10‰). This suggests that
237 some hydrothermal processes, such as phase separation and Hg redox reactions, cause less MDF in
238 submarine hydrothermal systems than in subaerial hydrothermal systems.^{19, 65, 66}

239 The Hg isotopic compositions in submarine hydrothermal sulfides have been interpreted to reflect a
240 mixture of primordial (magmatic/mantle) Hg and seawater Hg under a regime of hydrothermal leaching^{15, 60}.
241 The magmatic/mantle Hg is characterized by zero MIF^{64, 68}, and the seawater Hg typically by small and
242 positive MIF^{33, 69}. Using a binary mixing model which assumes magmatic/mantle and open seawater have
243 mean $\Delta^{199}\text{Hg}$ values of $0.00 \pm 0.05\text{‰}$ ⁶⁴ and $0.11 \pm 0.09\text{‰}$ (1SD, represented by Atlantic open seawater)³³,
244 respectively, we estimate that on average ~50% of Hg in CIR sulfides (Edmond and Kairei: 46%, 34-73%)
245 and SWIR sulfides (Duanqiao: 46%, 40-59%; Longqi: 51%, 37-75%; Yuhuang: 49%, 33-82%; respectively)
246 sourced from seawater. We acknowledge that the calculated seawater Hg contributions to the sulfides are
247 biased by the representativeness of magmatic/mantle and open seawater end-members, and potentially small
248 MIF during the abiotic, hydrothermal processes⁷⁰. Even though, seafloor sulfide deposits could be an
249 important sink of seawater Hg as well as hydrothermal Hg in deep oceans. In addition, the regression slope
250 of $\Delta^{199}\text{Hg}$ and $\Delta^{201}\text{Hg}$ line (1.04 ± 0.08 ; 1SE) for all Indian Ocean Ridge sulfide samples (Figure S2)
251 suggests that odd-MIF in the hydrothermal sulfides was imparted by seawater that transported to depth
252 following Hg(II) photo-reduction at the ocean surface²².

253 The total accumulation of seafloor sulfide deposits in global submarine neovolcanic zones is estimated
254 as $\sim 6 \times 10^8$ Mg, and sulfides on slow- and ultra-slow spreading centers (spreading rate < 40 mm yr^{-1})
255 including Indian Ocean Ridge account for $\sim 86\%$ of the total mass of sulfide deposits at ridges^{71,72}. Based
256 on the mean Hg concentration (4475 ± 6400 ng g^{-1} , $n = 56$) of massive sulfides in four HFs (Table 1) we
257 calculated that the seafloor hydrothermal sulfides deposited 2685 ± 3840 Mg of Hg, in which ~ 1300 Mg
258 from seawater according to our binary mixing model. A recent study estimated that the total Hg budget in
259 global mid-ocean ridge regions could reach ~ 320 Mg yr^{-1} ⁶⁰, implying that seawater and magmatic/mantle
260 Hg, each of ~ 160 Mg yr^{-1} , are immobilized in seafloor sulfide deposits. The seawater Hg sink fluxes via
261 seafloor hydrothermal sulfides are thus equally important as those via trench sediments, also estimated as
262 ~ 160 Mg yr^{-1} ⁷³. It is interesting to note that trench sediments mainly remove anthropogenic Hg sinking
263 from surface to trench waters⁷³, while hydrothermal sulfides appear to mainly remove natural Hg of deep
264 oceans¹². Taken together, the seawater Hg removal via seafloor hydrothermal sulfides and trench sediments
265 could reach 320 Mg yr^{-1} . These fluxes are not explicitly included in the most recent Global Mercury
266 Assessment report by UNEP¹⁶, which estimated ~ 600 Mg yr^{-1} Hg removal via deep-sea sediments and ~ 200
267 Mg yr^{-1} Hg removal via coastal sediments.

268 **3.2. Limited MIF Values in Chemosynthetic Food Webs**

269 Relative to most of the deep-sea environments, hydrothermal fields and cold seeps often host large
270 biomass and productivity. The biota (mostly macroinvertebrates including crabs, snails, shrimps, mussels)
271 surrounding hydrothermal fields are adapted to wide temperature range, and typically possess symbiotic
272 relationships with chemoautotrophs that convert the dissolved chemicals from the vent fluids into organic
273 matter⁷⁴. The stable isotopic compositions of carbon and nitrogen ($\delta^{13}\text{C}$ and $\delta^{15}\text{N}$) are generally used to
274 determine the origin of food sources (organic matter) and biosynthetic pathways. The $\delta^{13}\text{C}$ and $\delta^{15}\text{N}$ values
275 in our hydrothermal biota were quite variable, ranging from -36.28 to -13.63% and -12.04 to 8.69% ,

276 respectively. These values are within the ranges ($\delta^{13}\text{C}$: -36.91 to -8.29‰; $\delta^{15}\text{N}$: -15.8 to 11.78‰) of
277 counterparts collected around Mid-Atlantic Ridge hydrothermal vent fields⁷⁵. Within the same species, they
278 have similar $\delta^{13}\text{C}$ and $\delta^{15}\text{N}$ values, with highest values for shrimps ($\delta^{13}\text{C}$: -13.70 to -13.63‰; $\delta^{15}\text{N}$: 7.74 to
279 8.69‰), intermediate values for crabs ($\delta^{13}\text{C}$: -18.73 to -16.27‰; $\delta^{15}\text{N}$: 6.84 to 7.91‰) and “scaly-foot”
280 gastropods ($\delta^{13}\text{C}$: -23.47‰; $\delta^{15}\text{N}$: 4.95‰) and lowest values for mussels ($\delta^{13}\text{C}$: -36.28 to -31.82‰; $\delta^{15}\text{N}$:
281 -12.04 to 0.39‰) (Table S2, Figure 4). The lowest $\delta^{13}\text{C}$ values of our mussels overlapped with those
282 observed for different species of mussels from Mid-Atlantic Ridge and Pacific hydrothermal vents, known
283 to host thiotrophic symbionts⁷⁵⁻⁷⁷. These symbiotic autotrophic bacteria are also accountable for the lowest
284 $\delta^{15}\text{N}$ values in the mussels by providing local nutrients for the hosts⁷⁸. The shrimps with both the highest
285 $\delta^{13}\text{C}$ and $\delta^{15}\text{N}$ had much higher $\delta^{13}\text{C}$ than deep-sea surface sediments and pelagic particulate organic matter
286 sinking from the euphotic zone (ca. between -28‰ and -19‰) (Figure 4-a)^{79, 80}, suggesting that sinking
287 particles does not constitute a substantial part of their diet. The crabs and “scaly-foot” gastropod with
288 intermediate $\delta^{13}\text{C}$ and $\delta^{15}\text{N}$ values likely suggests their mixed food sources.

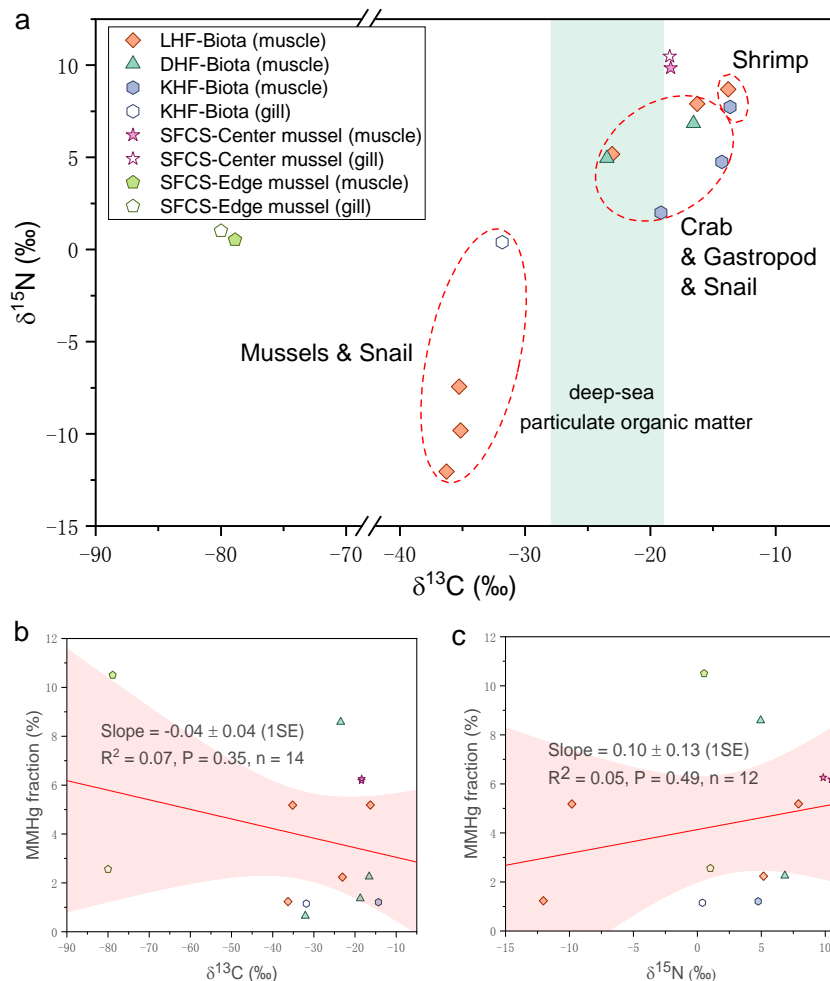


Figure 4. Plots of $\delta^{15}\text{N}$ versus $\delta^{13}\text{C}$ (a), MMHg% versus $\delta^{13}\text{C}$ (b), and MMHg% versus $\delta^{15}\text{N}$ (c) in hydrothermal biota from different hydrothermal fields at the Indian Ocean Ridge and mussels from the Site F cold seep at the South China Sea. Note LHF: Longqi HF; DHF: Duanqiao HF; KHF: Kairei HF; SFCS-Center mussel: mussel near the center of Site F cold seep; SFCS-Edge mussel: mussel at the edge of Site F cold seep. The typical $\delta^{13}\text{C}$ range is shown in the green shaded area for deep-sea particulate organic matter^{79, 80}.

Our hydrothermal biota had a wide range of THg concentrations (6.0 to 7045 ng g^{-1} , $928 \pm 1883 \text{ ng g}^{-1}$; dry weight, $n = 16$). On average, THg concentrations in biota were highest in Duanqiao HF, SWIR (164 to 7045 ng g^{-1} ; $2488 \pm 2950 \text{ ng g}^{-1}$; $n = 5$), which were ~ 10 times higher ($P < 0.05$) than those in nearby Longqi HF (6.0 to 882 ng g^{-1} , $261 \pm 311 \text{ ng g}^{-1}$; $n = 7$) and ~ 20 times higher ($P = 0.06$) than Kairei HF, CIR (9.3 to 307 ng g^{-1} , $142 \pm 156 \text{ ng g}^{-1}$; $n = 4$) (Table 1). In addition to sampling bias in the types of biota samples, this large difference likely also reflected the variability of THg concentrations in hydrothermal fluids and sulfides (Figure 2; Table 1). THg concentrations are lowest in CIR but are comparatively high in SWIR for both sulfides ($P = 0.31$) and biota ($P = 0.35$). Similar observations were also made in previous studies which

304 showed that hydrothermal sulfides and biota from the active hydrothermal vents of Tonga Arc in
305 southwestern Pacific were orders of magnitude higher than those in Mid-Atlantic Ridge ^{11, 81, 82}. MMHg
306 concentrations in the hydrothermal biota also varied largely (2.7 to 53.1 ng g⁻¹) but only accounted for very
307 small fractions of THg concentrations (~3%, mostly <10%). Even smaller fractions (<1%) of MMHg were
308 observed in hydrothermal biota of Tonga Arc and Mid-Atlantic Ridge ^{11, 81}. In contrast, MMHg in benthic
309 invertebrates living in coastal, hadal, fresh and abyssal environments are on average account for ~76%,
310 ~32%, ~21% and ~8% of THg, respectively ³⁹. The low MMHg fractions in hydrothermal biota are likely
311 related to the low MMHg discharge rate ¹⁸ and low Hg methylation in the hydrothermal vent environments
312 due to high temperature and limited bioavailability of Hg(II) for bacteria capable of methylation ^{11, 83}.
313 Besides, MMHg has been suggested to be rapidly demethylated in fluid plumes ¹². Further, symbiotic
314 chemoautotrophs hosted by hydrothermal biota might transform MMHg into inorganic Hg with temporary
315 detoxified storage and excretion in the digestive gland ⁸⁴, but the detoxification mechanism is unclear yet.
316 The absence of correlations between MMHg fractions and $\delta^{13}\text{C}$ or $\delta^{15}\text{N}$ values in our studied biota (Figure
317 4b-c) suggests that the food sources and trophic levels have a limited effect on the ultimate Hg accumulation
318 in the deep-sea hydrothermal ecosystems. The correlations between MMHg in our studied biota and food
319 sources is potentially obscured by various biogeochemical processes as listed above. The “scaly-foot”
320 gastropod known only from deep-sea hydrothermal vents in the Indian Ocean had the highest THg
321 concentrations (7045 ng g⁻¹ in Duanqiao HF and 882 ng g⁻¹ in Longqi HF) among all collected biota, with
322 MMHg concentrations up to 606 ng g⁻¹ (~8.6% of THg) in Duanqiao HF (Table S2). This is most likely due
323 to the use of iron sulfides (pyrite and greigite, typically enriched in Hg) in the structure of the dermal
324 sclerites of the “scaly-foot” gastropod, which may increase Hg levels in its body.

325 Overall, $\delta^{202}\text{Hg}$ and $\Delta^{199}\text{Hg}$ values of hydrothermal biota varied within small ranges, from -0.91 to 0.52‰
326 (mean = $-0.33 \pm 0.48\text{‰}$, n = 13) and 0.04 to 0.48‰ ($0.13 \pm 0.12\text{‰}$, n=13), respectively. On average, $\delta^{202}\text{Hg}$
327 in Duanqiao HF ($-0.12 \pm 0.59\text{‰}$, n = 5) was less negative than Kairei ($-0.27 \pm 0.42\text{‰}$, n = 3, p = 0.71) and

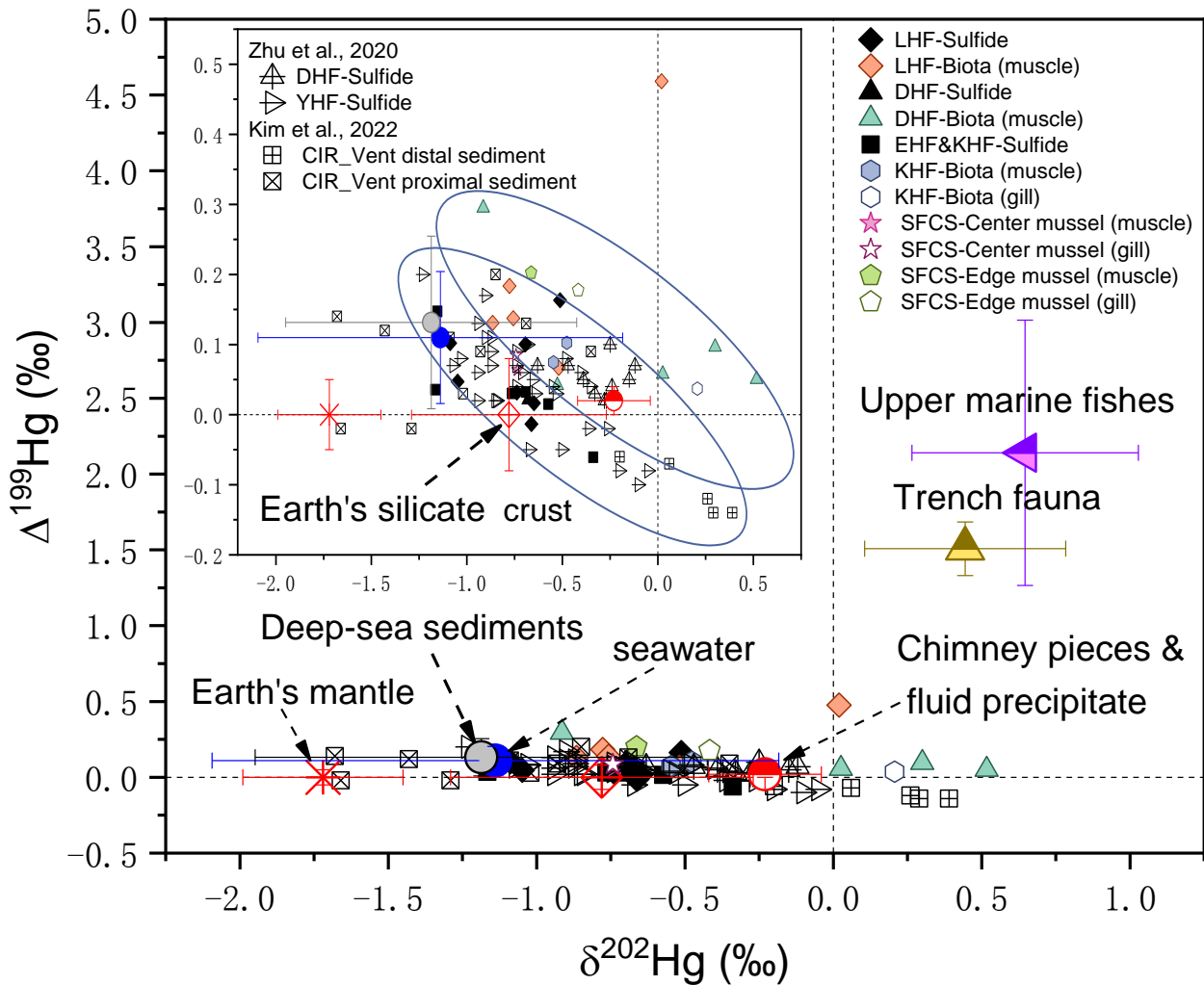
328 Longqi ($-0.58 \pm 0.36\text{‰}$, $n = 5$, $p = 0.18$) HF; $\Delta^{199}\text{Hg}$ was higher in Longqi HF ($0.20 \pm 0.16\text{‰}$, $n = 5$) than
329 Duanqiao ($0.11 \pm 0.11\text{‰}$, $n = 5$, $p = 0.15$) and Kairei ($0.07 \pm 0.03\text{‰}$, $n = 3$, $p = 0.07$) HF (Table 1).
330 Previous studies on coastal benthic invertebrates revealed similar $\Delta^{199}\text{Hg}$ values ($0.11 \pm 0.06\text{‰}$ for bivalve,
331 $0.18 \pm 0.11\text{‰}$ for shrimp, $0.20 \pm 0.14\text{‰}$ for cephalopod, $0.21 \pm 0.07\text{‰}$ for gastropod, and $0.25 \pm 0.07\text{‰}$ for
332 crab) but significantly lower $\delta^{202}\text{Hg}$ values (-2.05 to -1.49‰ , group-specific mean values)⁵². Increases of
333 both $\delta^{202}\text{Hg}$ and $\Delta^{199}\text{Hg}$ are seen from coastal/estuarine fishes^{52, 85} to open marine fishes³⁴⁻³⁷ and then to
334 mammals/birds⁸⁶⁻⁸⁸. As compared to their nearby sulfides, $\delta^{202}\text{Hg}$ and $\Delta^{199}\text{Hg}$ in our hydrothermal biota are
335 slightly shifted by 0.19 to 0.51‰ (site-specific means: Longqi: $0.19 \pm 0.42\text{‰}$, $P = 0.28$; Duanqiao: $0.23 \pm$
336 0.62‰ , $P = 0.44$; Kairei/Edmond: $0.51 \pm 0.53\text{‰}$, $P = 0.08$) and 0.04 to 0.14‰ (site-specific means: Longqi:
337 $0.14 \pm 0.17\text{‰}$, $P = 0.07$; Duanqiao: $0.06 \pm 0.11\text{‰}$, $P = 0.22$; Kairei/ Edmond: $0.04 \pm 0.07\text{‰}$, $P = 0.43$),
338 respectively. These positive shifts of $\delta^{202}\text{Hg}$ and $\Delta^{199}\text{Hg}$ could be caused by bioaccumulation and trophic
339 transfer of MMHg⁸⁹⁻⁹¹. However, the lack of significant correlations of MMHg% with $\delta^{202}\text{Hg}$ and $\Delta^{199}\text{Hg}$
340 (Figure S3) exclude this possibility. Alternatively, these shifts are more likely caused by the assimilation of
341 seawater Hg (characterized by higher $\Delta^{199}\text{Hg}$ values)⁹² into biota and the precipitation of sulfides from
342 hydrothermal fluids which could increase $\delta^{202}\text{Hg}$ values of discharged hydrothermal fluids^{93, 94}.

343 Like hydrothermal fields, cold seeps also host many organisms symbiotic with chemoautotrophs that
344 use the methane and hydrogen sulfide present in the seep water as an energy source. Cold seeps occur
345 mostly at tectonic plate boundaries, and thus might release Hg into seawater as well. According to our
346 mussel samples from the Site F deep cold seep in the South China Sea, the bathymodiolin mussel
347 *Bathymodiolus adulooides* (near the center of cold seep) with higher Hg concentrations (592 to 920 ng g^{-1})
348 had lower $\delta^{202}\text{Hg}$ (-0.74 to -0.73‰) and $\Delta^{199}\text{Hg}$ (0.06 to 0.08‰); another *Gigantidas platifrons* (at the edge
349 of the cold seep) with lower Hg concentrations (46 to 173 ng g^{-1}) had slightly higher $\delta^{202}\text{Hg}$ (-0.66 to
350 -0.42‰) and $\Delta^{199}\text{Hg}$ (0.18 to 0.20‰) (Table S2, Figure S4). Overall, their Hg concentrations and isotopic
351 compositions are comparable to those of hydrothermal biota. Insignificant differences (0.13‰ for $\delta^{202}\text{Hg}$

352 and 0.02‰ for $\Delta^{199}\text{Hg}$) in Hg isotopic compositions are observed between the gill and muscle of the mussels,
353 although THg concentrations are significantly higher in the gill (Table S2). The fractions of MMHg in
354 mussels from the Site F cold seep are also very low (2.6-10.5%).

355 **3.3. Sources of Hg in Chemosynthetic Food Webs**

356 The Hg isotope signature $\Delta^{199}\text{Hg}$ has been used as a robust tracer of Hg sources of marine food webs³⁰,
357 ³¹. $\Delta^{199}\text{Hg}$ values of MMHg in the upper oceans are significantly positive (0.82 to 5.50‰, $2.14 \pm 0.87\%$;
358 $n=137$; Figure 5) as proxied by pelagic fishes and decrease systematically with increasing depths³⁴⁻³⁷. The
359 $\Delta^{199}\text{Hg}$ values of inorganic Hg as inferred from seawater (mean values: 0.07‰ for Mediterranean Sea; 0.11‰
360 for Atlantic) and suspended particles (Mediterranean Sea: -0.06‰; Atlantic: -0.21‰; Pacific: 0.16‰) in
361 upper oceans are consistently small and show limited variations toward deep oceans as inferred from
362 sediments (Mediterranean Sea: 0.09‰; Atlantic: 0.01‰; Pacific: 0.29‰)³³. Although the difference of
363 $\delta^{202}\text{Hg}$ between MMHg and inorganic Hg in upper oceans is not as remarkable as $\Delta^{199}\text{Hg}$, $\delta^{202}\text{Hg}$ values of
364 MMHg are mainly positive (-0.43 to 1.84‰, $0.65 \pm 0.38\%$; $n=137$; Figure 5), in contrast to $\delta^{202}\text{Hg}$ values of
365 inorganic Hg that are dominantly negative (mean values: -0.27‰ for seawater; -0.28‰ for suspend particles)
366 ³³. Two studies on hadal amphipods and snailfish from the deepest oceans (Kermadec and Mariana
367 trenches, >6000 m) found that their Hg isotopic compositions ($\delta^{202}\text{Hg} = 0.44 \pm 0.34\%$, $\Delta^{199}\text{Hg} = 1.51 \pm$
368 0.18% , $n=59$; Figure 5) closely matched those of MMHg in upper oceans and suggested that their Hg
369 mostly derived from bioavailable MMHg in upper marine food webs via sinking particles and carrion^{38,40}.
370 The significantly lower $\Delta^{199}\text{Hg}$ values in our epibenthic biota (0.04 to 0.48‰) of hydrothermal fields and
371 cold seeps (0.06 to 0.20‰) (Figure 5) suggest there is little to no upper marine MMHg in deep-sea
372 chemosynthetic food webs that mainly rely on symbiotic chemoautotrophs for food and energy.



373

374 **Figure 5.** $\Delta^{199}\text{Hg}$ versus $\delta^{202}\text{Hg}$ in biota (including two samples from the Site F cold seep, abbreviated as
 375 SFCS, South China Sea), sulfides and sediments from Indian Ocean Ridge reported in this and previous
 376 studies^{15,60}. Also shown are Hg isotope values (mean \pm 1SD) of chimney pieces and fluid precipitate from
 377 Guaymas Basin (filled red-white circle)¹⁹, Earth's silicate crust (empty red diamond)⁶², primordial mantle
 378 (red cross)⁶⁴, seawater (filled blue circle)^{33,69}, deep-sea (>1000 m) sediments (filled gray circle)^{33,38,73,}
 379 ⁹⁵⁻⁹⁸, trench fauna (filled brown-yellow triangle)^{38,40}, and upper marine fishes (filled purple-pink triangle)
 380 ³³⁻³⁷. The inset shows the enlarged area of the figure, and the ellipses are used to outline the variation ranges
 381 of Hg isotopic compositions for sulfides/sediments and biota.

382

383 Large amounts of Hg could be discharged from the surrounding hydrothermal vents^{18,19}. Although Hg
 384 isotopic compositions in submarine hydrothermal fluids have not been reported, their MIF values are
 385 expected to be conserved in fluid precipitates and deposited sulfides due to lack of MIF inducing processes.
 386 As shown above, $\Delta^{199}\text{Hg}$ values in hydrothermal biota (0.07 to 0.20‰, location-specific means) were
 387 slightly and positively shifted relative to their nearby sulfides (0.03 to 0.06‰, location-specific means), thus
 388 the original hydrothermal fluids, implying that Hg from ambient seawater with higher $\Delta^{199}\text{Hg}$ values (up to
 0.4‰)^{33,69} were also incorporated into hydrothermal food webs. It appears that the hydrothermal Hg

389 contributions to food webs were more important in Duanqao HF than Longqi HF, because the $\Delta^{199}\text{Hg}$ shifts
390 between biota and sulfides in the former (0.06‰) are about two times smaller than the latter (0.14‰)
391 (Table1, Figure 3). This inference is also supported by the ~10 times higher ($P < 0.05$) Hg concentrations in
392 biota from Duanqao HF than Longqi HF.

393 It is still unknown if the studied cold seep was releasing Hg during the sampling period. As shown in
394 Figure S4, a previous study found no statistical difference in THg and MMHg concentrations and Hg
395 isotopic compositions between sediments from a cold seep in the northern Gulf of Mexico ($\delta^{202}\text{Hg} = -0.72 \pm$
396 0.11‰ , $\Delta^{199}\text{Hg} = 0.08 \pm 0.03\text{‰}$, $n = 7$) and from background sites ($\delta^{202}\text{Hg} = -0.66 \pm 0.10\text{‰}$; $\Delta^{199}\text{Hg} = 0.06$
397 $\pm 0.02\text{‰}$; $n = 5$), and suggested that cold seeps are not significant sources of Hg. Our near-field mussel
398 with >5 times higher Hg concentration had comparable Hg isotopic compositions ($\delta^{202}\text{Hg}$: -0.74 to -0.73‰;
399 $\Delta^{199}\text{Hg}$: 0.06 to 0.08‰) to these values. Our far-field mussel with lower Hg concentration had slightly
400 higher $\delta^{202}\text{Hg}$ (-0.66 to -0.42‰) and $\Delta^{199}\text{Hg}$ (0.18 to 0.20‰), with the $\Delta^{199}\text{Hg}$ is close to the background
401 sediment values (0.21 to 0.45‰) from the South China Sea ⁹⁶. Given that $\Delta^{199}\text{Hg}$ values of geogenic Hg
402 released from the cold seep are most likely close to 0‰, the higher Hg concentrations and lower $\Delta^{199}\text{Hg}$
403 values of the near-field mussel implies that the cold seep was likely releasing Hg to the ambient environment.
404 However, Hg isotopic compositions in more cold seep biota samples and co-located sediments and seawater
405 are still needed for confirmation.

406 The biota samples in our studied hydrothermal fields and cold seep contained small fractions (<10%) of
407 MMHg which show insignificant correlations with $\delta^{202}\text{Hg}$ and $\Delta^{199}\text{Hg}$ (Figure S3), suggesting that the Hg
408 isotope values between MMHg and inorganic Hg are not significantly different, and that the MMHg in these
409 biota samples were likely derived from *in situ* methylation of inorganic Hg surrounding the hydrothermal
410 fields and cold seep rather than MMHg transported from upper oceans. This is because upper marine MMHg
411 have significantly higher $\delta^{202}\text{Hg}$ and $\Delta^{199}\text{Hg}$ than deep marine inorganic Hg (Figure 5), we would expect an

412 increase of $\delta^{202}\text{Hg}$ and $\Delta^{199}\text{Hg}$ with the increasing fractions of upper marine MMHg (see Figure S3 for the
413 theoretical mixing lines between deep marine inorganic Hg and upper marine MMHg). Previous studies
414 found small fractions of MMHg in sediments near hydrothermal fields (<0.1%)¹¹ and cold seeps (~2.4%)¹⁴,
415 which might partly explain the higher ($p = 0.02$) MMHg fractions in biota from cold seeps than
416 hydrothermal fields. It is noted that our inference on MMHg isotope compositions is likely biased by the low
417 MMHg fractions of our samples which do not show sufficient variation. MMHg from upper oceans could
418 possibly incorporate into some biota (e.g., SY128-gastropod of very high $\Delta^{199}\text{Hg}$), but its isotope signatures
419 were overwhelmed by those of inorganic Hg. More work (e.g., species-specific MMHg isotope analysis) is
420 still needed to decipher the sources of MMHg in chemosynthetic food webs.

421 **4. Implications**

422 Our results have important implications for understanding the Hg cycling in deep oceans. First, the Hg
423 isotopic compositions in the submarine hydrothermal sulfides suggest seawater Hg removal flux by sulfides
424 is potentially significant, but more work is still needed to constrain this flux. If these additional Hg removal
425 fluxes are implemented in future models, the turnover time of seawater Hg and the clearance time of
426 anthropogenic Hg are expected to be much shorter than previously estimated. Second, there are still
427 technical challenges to directly measure seawater Hg isotopes³³, especially for the deep oceans. The
428 measurement of Hg isotopic compositions in biota living at different sea-floor environments would serve as
429 a promising tool to understand the sources and biogeochemical cycling of deep-sea Hg. Our first
430 measurement of Hg isotopic compositions of epibenthic biota from hydrothermal fields and cold seeps
431 indicates that the Hg in chemosynthetic food webs is almost exclusively sourced from hydrothermal fluids
432 and ambient seawater Hg, with little to no contribution from MMHg in photosynthetic food webs of upper
433 oceans. In contrast, previous studies showed that the Hg in trench food webs was mostly derived from
434 photosynthetic food webs^{38,40}. This contrast reflects the remarkable difference in the ways how the energy

435 and food were gained among different deep-sea ecosystems. While our studied hydrothermal fields and cold
436 seeps are rather deep, future studies on chemosynthetic food webs at shallower depths and food webs at
437 seamounts and abyssal plains may help understand the interaction of chemosynthetic and photosynthetic
438 food webs.

439 ASSOCIATED CONTENT

440 Supporting Information

441 Additional details about study area, THg and MMHg concentrations, and Hg isotope analysis, figures, and
442 tables.

443 AUTHOR INFORMATION

444 Notes

445 The authors declare no competing financial interest.

446 ACKNOWLEDGMENTS

447 Funding for this research was provided by the National Natural Science Foundation of China (42173011 and
448 11975247), the Major Consulting Project of Academy-local Cooperation of Chinese Academy of
449 Engineering (2021DFZD2), the Tianjin Natural Science Foundation (20JCQNJC01650), and the French
450 National Funding Agency Project HydrOThermal Mercury (ANR-21-CE34-0026). J. Yuan acknowledges
451 her PhD scholarship from the Chinese Scholar Council (File No. 202106250118). The authors are grateful to
452 the pilots, the captain, and crew of the R/V Tansuoyihao with the manned submersible Shenhai Yongshi for
453 their professional service during the TS10 cruise. The authors thank the captains, crew, and sampling teams
454 including D. Feng and L. Zhang of the cruises in the South China Sea. The authors also thank the Editor and
455 four anonymous reviewers for their insightful suggestions and comments.

457 **REFERENCES**

- 458 1. Outridge, P. M.; Mason, R. P.; Wang, F.; Guerrero, S.; Heimbürger-Boavida, L. E., Updated Global and Oceanic Mercury
459 Budgets for the United Nations Global Mercury Assessment 2018. *Environ. Sci. Technol.* **2018**, *52*, 11466-11477.
- 460 2. Mason, R. P.; Choi, A. L.; Fitzgerald, W. F.; Hammerschmidt, C. R.; Lamborg, C. H.; Soerensen, A. L.; Sunderland, E. M.,
461 Mercury biogeochemical cycling in the ocean and policy implications. *Environ. Res.* **2012**, *119*, 101-117.
- 462 3. Bowman, K. L.; Lamborg, C. H.; Agather, A. M., A global perspective on mercury cycling in the ocean. *Sci. Total Environ.*
463 **2020**, *710*, 136166.
- 464 4. Cui, X.; Lamborg, C. H.; Hammerschmidt, C. R.; Xiang, Y.; Lam, P. J., The Effect of Particle Composition and
465 Concentration on the Partitioning Coefficient for Mercury in Three Ocean Basins. *Front. Environ. Chem.* **2021**, *2*, 660267.
- 466 5. Lamborg, C. H.; Hammerschmidt, C. R.; Bowman, K. L., An examination of the role of particles in oceanic mercury cycling.
467 *Philos. Trans. A. Math. Phys. Eng. Sci.* **2016**, *374*, 20150297.
- 468 6. Lamborg, C. H.; Hammerschmidt, C. R.; Bowman, K. L.; Swarr, G. J.; Munson, K. M.; Ohnemus, D. C.; Lam, P. J.;
469 Heimbürger, L. E.; Rijkenberg, M. J.; Saito, M. A., A global ocean inventory of anthropogenic mercury based on water column
470 measurements. *Nature* **2014**, *512*, 65-8.
- 471 7. Jamieson, A. J.; Malkocs, T.; Piertney, S. B.; Fujii, T.; Zhang, Z., Bioaccumulation of persistent organic pollutants in the
472 deepest ocean fauna. *Nat. Ecol. Evol.* **2017**, *1*, 1-4.
- 473 8. Heimbürger, L.-E.; Cossa, D.; Thibodeau, B.; Khripounoff, A.; Mas, V.; Chiffolleau, J.-F.; Schmidt, S.; Migon, C., Natural
474 and anthropogenic trace metals in sediments of the Ligurian Sea (Northwestern Mediterranean). *Chem. Geol.* **2012**, *291*, 141-151.
- 475 9. Gobeil, C.; Macdonald, R. W.; Smith, J. N., Mercury Profiles in Sediments of the Arctic Ocean Basins. *Environ. Sci. Technol.*
476 **1999**, *33*, 4194-4198.
- 477 10. German, C. R.; Casciotti, K. A.; Dutay, J. C.; Heimbürger, L. E.; Jenkins, W. J.; Measures, C. I.; Mills, R. A.; Obata, H.;
478 Schlitzer, R.; Tagliabue, A.; Turner, D. R.; Whitby, H., Hydrothermal impacts on trace element and isotope ocean biogeochemistry.
479 *Philos. Trans. A. Math. Phys. Eng. Sci.* **2016**, *374*, 20160035.
- 480 11. Lee, S.; Kim, S. J.; Ju, S. J.; Pak, S. J.; Son, S. K.; Yang, J.; Han, S., Mercury accumulation in hydrothermal vent mollusks
481 from the southern Tonga Arc, southwestern Pacific Ocean. *Chemosphere* **2015**, *127*, 246-53.
- 482 12. Lamborg, C. H.; Von Damm, K. L.; Fitzgerald, W. F.; Hammerschmidt, C. R.; Zierenberg, R., Mercury and
483 monomethylmercury in fluids from Sea Cliff submarine hydrothermal field, Gorda Ridge. *Geophys. Res. Lett.* **2006**, *33*, L17606.
- 484 13. Cossa, D.; Knoery, J.; Banaru, D.; Harmelin-Vivien, M.; Sonke, J. E.; Hedgecock, I. M.; Bravo, A. G.; Rosati, G.; Canu, D.;
485 Horvat, M.; Sprovieri, F.; Pirrone, N.; Heimbürger-Boavida, L. E., Mediterranean Mercury Assessment 2022: An Updated Budget,
486 Health Consequences, and Research Perspectives. *Environ. Sci. Technol.* **2022**, *56*, 3840-3862.
- 487 14. Brown, G., Jr.; Sleeper, K.; Johnson, M. W.; Blum, J. D.; Cizdziel, J. V., Mercury concentrations, speciation, and isotopic
488 composition in sediment from a cold seep in the northern Gulf of Mexico. *Mar. Pollut. Bull.* **2013**, *77*, 308-14.
- 489 15. Zhu, C.; Tao, C.; Yin, R.; Liao, S.; Yang, W.; Liu, J.; Barriga, F. J. A. S., Seawater versus mantle sources of mercury in
490 sulfide-rich seafloor hydrothermal systems, Southwest Indian Ridge. *Geochim. Cosmochim. Acta* **2020**, *281*, 91-101.
- 491 16. UN-Environment, Global Mercury Assessment 2018. UN Environment Programme, Chemicals and Health Branch Geneva,
492 Switzerland. **2019**.
- 493 17. UN-Environment, Global Mercury Assessment 2013: Sources, Emissions, Releases and Environmental Transport. UNEP
494 Chemicals Branch, Geneva, Switzerland. **2013**.
- 495 18. Crepo-Medina, M.; Chatziefthimiou, A. D.; Bloom, N. S.; Luther, G. W. I.; Wright, D. D.; Reinfelder, J. R.; Vetriani, C.;
496 Barkay, T., Adaptation of chemosynthetic microorganisms to elevated mercury concentrations in deep-sea hydrothermal vents.
497 *Limnol. Oceanogr.* **2009**, *54*, 41-49.
- 498 19. Sherman, L. S.; Blum, J. D.; Nordstrom, D. K.; McCleskey, R. B.; Barkay, T.; Vetriani, C., Mercury isotopic composition of
499 hydrothermal systems in the Yellowstone Plateau volcanic field and Guaymas Basin sea-floor rift. *Earth Planet. Sci. Lett.* **2009**,
500 *279*, 86-96.

- 501 20. Blum, J. D.; Sherman, L. S.; Johnson, M. W., Mercury Isotopes in Earth and Environmental Sciences. In *Annual Review of*
502 *Earth and Planetary Sciences*, Jeanloz, R., Ed. 2014; Vol. 42, pp 249-269.
- 503 21. Sun, R.; Jiskra, M.; Amos, H. M.; Zhang, Y.; Sunderland, E. M.; Sonke, J. E., Modelling the mercury stable isotope
504 distribution of Earth surface reservoirs: Implications for global Hg cycling. *Geochim. Cosmochim. Acta* **2019**, *246*, 156-173.
- 505 22. Bergquist, B. A.; Blum, J. D., Mass-dependent and -independent fractionation of Hg isotopes by photoreduction in aquatic
506 systems. *Science* **2007**, *318*, 417-420.
- 507 23. Zheng, W.; Hintelmann, H., Mercury isotope fractionation during photoreduction in natural water is controlled by its
508 Hg/DOC ratio. *Geochim. Cosmochim. Acta* **2009**, *73*, 6704-6715.
- 509 24. Kritee, K.; Motta, L. C.; Blum, J. D.; Tsui, M. T.-K.; Reinfelder, J. R., Photomicrobial Visible Light-Induced Magnetic Mass
510 Independent Fractionation of Mercury in a Marine Microalga. *ACS Earth Space Chem.* **2018**, *2*, 432-440.
- 511 25. Chandan, P.; Ghosh, S.; Bergquist, B. A., Mercury isotope fractionation during aqueous photoreduction of
512 monomethylmercury in the presence of dissolved organic matter. *Environ. Sci. Technol.* **2015**, *49*, 259-67.
- 513 26. Chen, J.; Hintelmann, H.; Feng, X.; Dimock, B., Unusual fractionation of both odd and even mercury isotopes in
514 precipitation from Peterborough, ON, Canada. *Geochim. Cosmochim. Acta* **2012**, *90*, 33-46.
- 515 27. Sun, G.; Sommar, J.; Feng, X.; Lin, C.-J.; Ge, M.; Wang, W.; Yin, R.; Fu, X.; Shang, L., Mass-Dependent and -Independent
516 Fractionation of Mercury Isotope during Gas-Phase Oxidation of Elemental Mercury Vapor by Atomic Cl and Br. *Environ. Sci.*
517 *Technol.* **2016**, *50*, 9232-9241.
- 518 28. Fu, X.; Jiskra, M.; Yang, X.; Maruszczak, N.; Enrico, M.; Chmeleff, J.; Heimburger-Boavida, L. E.; Gheusi, F.; Sonke, J. E.,
519 Mass-Independent Fractionation of Even and Odd Mercury Isotopes during Atmospheric Mercury Redox Reactions. *Environ. Sci.*
520 *Technol.* **2021**, *55*, 10164-10174.
- 521 29. Sun, G.; Feng, X.; Yin, R.; Wang, F.; Lin, C. J.; Li, K.; Sommar, J. O., Dissociation of Mercuric Oxides Drives Anomalous
522 Isotope Fractionation during Net Photo-oxidation of Mercury Vapor in Air. *Environ. Sci. Technol.* **2022**, *56*, 13428-13438.
- 523 30. Kwon, S. Y.; Blum, J. D.; Carvan, M. J.; Basu, N.; Head, J. A.; Madenjian, C. P.; David, S. R., Absence of fractionation of
524 mercury isotopes during trophic transfer of methylmercury to freshwater fish in captivity. *Environ. Sci. Technol.* **2012**, *46*,
525 7527-34.
- 526 31. Kwon, S. Y.; Blum, J. D.; Chirby, M. A.; Chesney, E. J., Application of mercury isotopes for tracing trophic transfer and
527 internal distribution of mercury in marine fish feeding experiments. *Environ. Toxicol. Chem.* **2013**, *32*, 2322-30.
- 528 32. Tsui, M. T.; Blum, J. D.; Kwon, S. Y., Review of stable mercury isotopes in ecology and biogeochemistry. *Sci. Total Environ.*
529 **2020**, *716*, 135386.
- 530 33. Jiskra, M.; Heimburger-Boavida, L. E.; Desgranges, M. M.; Petrova, M. V.; Dufour, A.; Ferreira-Araujo, B.; Masbou, J.;
531 Chmeleff, J.; Thyssen, M.; Point, D.; Sonke, J. E., Mercury stable isotopes constrain atmospheric sources to the ocean. *Nature*
532 **2021**, *597*, 678-682.
- 533 34. Blum, J. D.; Popp, B. N.; Drazen, J. C.; Choy, C. A.; Johnson, M. W., Methylmercury production below the mixed layer in
534 the North Pacific Ocean. *Nat. Geosci.* **2013**, *6*, 879-884.
- 535 35. Madigan, D. J.; Li, M.; Yin, R.; Baumann, H.; Snodgrass, O. E.; Dewar, H.; Krabbenhoft, D. P.; Baumann, Z.; Fisher, N. S.;
536 Balcom, P.; Sunderland, E. M., Mercury Stable Isotopes Reveal Influence of Foraging Depth on Mercury Concentrations and
537 Growth in Pacific Bluefin Tuna. *Environ. Sci. Technol.* **2018**, *52*, 6256-6264.
- 538 36. Motta, L. C.; Blum, J. D.; Popp, B. N.; Drazen, J. C.; Close, H. G., Mercury stable isotopes in flying fish as a monitor of
539 photochemical degradation of methylmercury in the Atlantic and Pacific Oceans. *Mar. Chem.* **2020**, *223*, 103790.
- 540 37. Motta, L. C.; Blum, J. D.; Johnson, M. W.; Umhau, B. P.; Popp, B. N.; Washburn, S. J.; Drazen, J. C.; Benitez - Nelson, C.
541 R.; Hannides, C. C. S.; Close, H. G.; Lamborg, C. H., Mercury Cycling in the North Pacific Subtropical Gyre as Revealed by
542 Mercury Stable Isotope Ratios. *Global Biogeochem. Cycles* **2019**, *33*, 777-794.
- 543 38. Sun, R.; Yuan, J.; Sonke, J. E.; Zhang, Y.; Zhang, T.; Zheng, W.; Chen, S.; Meng, M.; Chen, J.; Liu, Y.; Peng, X.; Liu, C.,
544 Methylmercury produced in upper oceans accumulates in deep Mariana Trench fauna. *Nat. Commun.* **2020**, *11*, 3389.
- 545 39. Liu, M.; Xiao, W.; Zhang, Q.; Shi, L.; Wang, X.; Xu, Y., Methylmercury Bioaccumulation in Deepest Ocean Fauna:
546 Implications for Ocean Mercury Biotransport through Food Webs. *Environ. Sci. Technol. Lett.* **2020**, *7*, 469-476.
- 547 40. Blum, J. D.; Drazen, J. C.; Johnson, M. W.; Popp, B. N.; Motta, L. C.; Jamieson, A. J., Mercury isotopes identify
548 near-surface marine mercury in deep-sea trench biota. *Proc. Natl. Acad. Sci. U.S.A.* **2020**, *117*, 29292-29298.

- 549 41. German, C. R.; Ramirez-Llodra, E.; Baker, M. C.; Tyler, P. A.; ChEss Scientific Steering, C., Deep-water chemosynthetic
550 ecosystem research during the census of marine life decade and beyond: a proposed deep-ocean road map. *PLoS One* **2011**, *6*,
551 e23259.
- 552 42. Feng, D.; Qiu, J.-W.; Hu, Y.; Peckmann, J.; Guan, H.; Tong, H.; Chen, C.; Chen, J.; Gong, S.; Li, N.; Chen, D., Cold seep
553 systems in the South China Sea: An overview. *J. Asian. Earth Sci.* **2018**, *168*, 3-16.
- 554 43. Bao, R.; Strasser, M.; McNichol, A. P.; Haghypour, N.; McIntyre, C.; Wefer, G.; Eglinton, T. I., Tectonically-triggered
555 sediment and carbon export to the Hadal zone. *Nat. Commun.* **2018**, *9*, 121.
- 556 44. Wang, N.; Shen, C.; Sun, W.; Ding, P.; Zhu, S.; Yi, W.; Yu, Z.; Sha, Z.; Mi, M.; He, L.; Fang, J.; Liu, K.; Xu, X.; Druffel, E.
557 R. M., Penetration of Bomb ¹⁴C Into the Deepest Ocean Trench. *Geophys. Res. Lett.* **2019**, *46*, 5413-5419.
- 558 45. Smith, J. K. L.; Ruhl, H. A.; Bettb, B. J.; Billett, D. S. M.; Lampitt, R. S.; Kaufmann, R. S., Climate, carbon cycling,
559 and deep-ocean ecosystems. *Proc. Natl. Acad. Sci. U.S.A.* **2009**, *106* 19211–19218.
- 560 46. Suess, E., Marine cold seeps and their manifestations: geological control, biogeochemical criteria and environmental
561 conditions. *Int. J. Earth Sci.* **2014**, *103*, 1889-1916.
- 562 47. McElhinny, M. W.; McFadden, P. L., Chapter Five - Oceanic Paleomagnetism. In *International Geophysics*, Academic Press:
563 2000; Vol. 73, pp 183-226.
- 564 48. Zhao, Y.; Xu, T.; Law, Y. S.; Feng, D.; Li, N.; Xin, R.; Wang, H.; Ji, F.; Zhou, H.; Qiu, J.-W., Ecological characterization of
565 cold-seep epifauna in the South China Sea. *Deep Sea Res. Part I Oceanogr. Res. Pap.* **2020**, *163*, 103361.
- 566 49. Feng, D.; Chen, D., Authigenic carbonates from an active cold seep of the northern South China Sea: New insights into fluid
567 sources and past seepage activity. *Deep Sea Res. Part II Top. Stud. Oceanogr.* **2015**, *122*, 74-83.
- 568 50. EPA-7473, Mercury in Solids and Solutions by Thermal Decomposition Amalgamation, and Atomic Absorption
569 Spectrophotometry. *USEPA* **2007**.
- 570 51. EPA-1630, Methyl Mercury in Water by Distillation, Aqueous Ethylation, Purge and Trap, and CVAFS. *USEPA* **2001**.
- 571 52. Meng, M.; Sun, R. Y.; Liu, H. W.; Yu, B.; Yin, Y. G.; Hu, L. G.; Chen, J. B.; Shi, J. B.; Jiang, G. B., Mercury isotope
572 variations within the marine food web of Chinese Bohai Sea: Implications for mercury sources and biogeochemical cycling. *J.*
573 *Hazard. Mater.* **2020**, *384*, 121379.
- 574 53. Zheng, W.; Gilleaudeau, G. J.; Kah, L. C.; Anbar, A. D., Mercury isotope signatures record photic zone euxinia in the
575 Mesoproterozoic ocean. *Proc. Natl. Acad. Sci. U. S. A.* **2018**, *115*, 10594-10599.
- 576 54. Chen, J.; Hintelmann, H.; Dimock, B., Chromatographic pre-concentration of Hg from dilute aqueous solutions for isotopic
577 measurement by MC-ICP-MS. *J. Anal. At. Spectrom.* **2010**, *25*, 1402-1409.
- 578 55. EPA-1631, Revision E: Mercury in Water by Oxidation, Purge and Trap, and Cold Vapor Atomic Fluorescence Spectrometry
579 *USEPA* **2002**.
- 580 56. Blum, J. D.; Bergquist, B. A., Reporting of variations in the natural isotopic composition of mercury. *Anal. Bioanal. Chem.*
581 **2007**, *388*, 353-359.
- 582 57. Blum, J. D.; Johnson, M. W., Recent developments in mercury stable isotope analysis. *Rev. Mineral. Geochem.* **2017**, *82*,
583 733-757.
- 584 58. Lee, J. H.; Kwon, S. Y.; Lee, H.; Nam, S.-I.; Kim, J.-H.; Joo, Y. J.; Jang, K.; Kim, H.; Yin, R., Climate-Associated Changes
585 in Mercury Sources in the Arctic Fjord Sediments. *ACS Earth Space Chem.* **2021**, *5*, 2398-2407.
- 586 59. Zheng, W.; Xie, Z.; Bergquist, B. A., Mercury Stable Isotopes in Ornithogenic Deposits As Tracers of Historical Cycling of
587 Mercury in Ross Sea, Antarctica. *Environ. Sci. Technol.* **2015**, *49*, 7623-32.
- 588 60. Kim, J.; Lim, D.; Jeong, D.; Xu, Z.; Kim, H.; Kim, J.; Kim, D., Mercury (Hg) geochemistry of mid-ocean ridge sediments on
589 the Central Indian Ridge: Chemical forms and isotopic composition. *Chem. Geol.* **2022**, *604*, 120942.
- 590 61. German, C. R.; Petersen, S.; Hannington, M. D., Hydrothermal exploration of mid-ocean ridges: Where might the largest
591 sulfide deposits be forming? *Chem. Geol.* **2016**, *420*, 114-126.
- 592 62. Sun, R.; Streets, D. G.; Horowitz, H. M.; Amos, H. M.; Liu, G.; Perrot, V.; Toutain, J.-P.; Hintelmann, H.; Sunderland, E. M.;
593 Sonke, J. E.; Blum, J. D.; Mason, R., Historical (1850–2010) mercury stable isotope inventory from anthropogenic sources to the
594 atmosphere. *Elem. Sci. Anth.* **2016**, *4*, 000091.
- 595 63. Zambardi, T.; Sonke, J. E.; Toutain, J. P.; Sortino, F.; Shinohara, H., Mercury emissions and stable isotopic compositions at
596 Vulcano Island (Italy). *Earth Planet. Sci. Lett.* **2009**, *277*, 236-243.

- 597 64. Moynier, F.; Jackson, M. G.; Zhang, K.; Cai, H.; Halldórsson, S. A.; Pik, R.; Day, J. M. D.; Chen, J., The Mercury Isotopic
598 Composition of Earth's Mantle and the Use of Mass Independently Fractionated Hg to Test for Recycled Crust. *Geophys. Res. Lett.*
599 **2021**, *48*, e2021GL094301.
- 600 65. Smith, C. N.; Kesler, S. E.; Klaue, B.; Blum, J. D., Mercury isotope fractionation in fossil hydrothermal systems. *Geology*
601 **2005**, *33*, 825-828.
- 602 66. Smith, C. N.; Kesler, S. E.; Blum, J. D.; Rytuba, J. J., Isotope geochemistry of mercury in source rocks, mineral deposits and
603 spring deposits of the California Coast Ranges, USA. *Earth Planet. Sci. Lett.* **2008**, *269*, 399-407.
- 604 67. Tang, Y.; Bi, X.; Yin, R.; Feng, X.; Hu, R., Concentrations and isotopic variability of mercury in sulfide minerals from the
605 Jinding Zn-Pb deposit, Southwest China. *Ore Geol. Rev* **2017**, *90*, 958-969.
- 606 68. Yin, R.; Chen, D.; Pan, X.; Deng, C.; Chen, L.; Song, X.; Yu, S.; Zhu, C.; Wei, X.; Xu, Y.; Feng, X.; Blum, J. D.; Lehmann,
607 B., Mantle Hg isotopic heterogeneity and evidence of oceanic Hg recycling into the mantle. *Nat. Commun.* **2022**, *13*, 948.
- 608 69. Štok, M.; Baya, P. A.; Hintelmann, H., The mercury isotope composition of Arctic coastal seawater. *C. R. Geosci.* **2015**, *347*,
609 368-376.
- 610 70. Zheng, W.; Hintelmann, H. J. T. J. o. P. C. A., Nuclear field shift effect in isotope fractionation of mercury during abiotic
611 reduction in the absence of light. **2010**, *114*, (12), 4238-4245.
- 612 71. Yu, J.; Tao, C.; Liao, S.; Alveirinho Dias, Á.; Liang, J.; Yang, W.; Zhu, C., Resource estimation of the sulfide-rich deposits of
613 the Yuhuang-1 hydrothermal field on the ultraslow-spreading Southwest Indian Ridge. *Ore Geol. Rev* **2021**, *134*, 104169.
- 614 72. Hannington, M.; Jamieson, J.; Monecke, T.; Petersen, S.; Beaulieu, S., The abundance of seafloor massive sulfide deposits.
615 *Geology* **2011**, *39*, 1155-1158.
- 616 73. Liu, M.; Xiao, W.; Zhang, Q.; Yuan, S.; Raymond, P. A.; Chen, J.; Liu, J.; Tao, S.; Xu, Y.; Wang, X., Substantial
617 accumulation of mercury in the deepest parts of the ocean and implications for the environmental mercury cycle. *Proc. Natl. Acad.*
618 *Sci. U. S. A.* **2021**, *118*, e2102629118.
- 619 74. Hoek, J.; Banta, A.; Hubler, F.; Reysenbach, A. L. J. G., Microbial diversity of a sulphide spire located in the Edmond deep
620 - sea hydrothermal vent field on the Central Indian Ridge. **2003**, *1*, (2), 119-127.
- 621 75. Colaço, A.; Dehairs, F.; Desbruyères, D., Nutritional relations of deep-sea hydrothermal fields at the Mid-Atlantic Ridge: a
622 stable isotope approach. *Deep Sea Res. Part I Oceanogr. Res. Pap.* **2002**, *49*, 395-412.
- 623 76. Dubilier, N.; Windoffer, R.; Giere, O., Ultrastructure and stable carbon isotope composition of the hydrothermal vent mussels
624 *Bathymodiolus brevior* and *B. sp. affinis brevior* from the North Fiji Basin, western Pacific. *Mar. Ecol. Prog. Ser.* **1998**, *165*,
625 187-193.
- 626 77. Pond, D. W.; Bell, M. V.; Dixon, D. R.; Fallick, A. E.; Segonzac, M.; Sargent, J. R., Stable-Carbon-Isotope Composition of
627 Fatty Acids in Hydrothermal Vent Mussels Containing Methanotrophic and Thiotrophic Bacterial Endosymbionts. *Appl. Environ.*
628 *Microbiol.* **1998**, *64*, 370-375.
- 629 78. Van Dover, C. L.; Fry, B., Stable isotopic compositions of hydrothermal vent organisms. *Mar. Biol.* **1989**, *102*, 257-263
- 630 79. Iken, K.; Bluhm, B. A.; Gradinger, R., Food web structure in the high Arctic Canada Basin: evidence from $\delta^{13}\text{C}$ and $\delta^{15}\text{N}$
631 analysis. *Polar Biology* **2004**, *28*, (3), 238-249.
- 632 80. Connelly, T. L.; Deibel, D.; Parrish, C. C., Biogeochemistry of near-bottom suspended particulate matter of the Beaufort Sea
633 shelf (Arctic Ocean): C, N, P, $\delta^{13}\text{C}$ and fatty acids. *Continental Shelf Research* **2012**, *43*, 120-132.
- 634 81. Martins, I.; Costa, V.; Porteiro, F.; Cravo, A.; Santos, R. S., Mercury concentrations in invertebrates from Mid-Atlantic Ridge
635 hydrothermal vent fields. *J. Mar. Biolog. Assoc. U.K.* **2001**, *81*, 913-915.
- 636 82. Demina, L. L.; Galkin, S. V., On the role of abiogenic factors in the bioaccumulation of heavy metals by the hydrothermal
637 fauna of the Mid-Atlantic Ridge. *Oceanology* **2008**, *48*, 784-797.
- 638 83. Lamborg, C. H.; Yigiterhan, O.; Fitzgerald, W. F.; Balcom, P. H.; Hammerschmidt, C. R.; Murray, J., Vertical distribution of
639 mercury species at two sites in the Western Black Sea. *Mar. Chem.* **2008**, *111*, 77-89.
- 640 84. Colaco, A.; Bustamante, P.; Fouquet, Y.; Sarradin, P. M.; Serrao-Santos, R., Bioaccumulation of Hg, Cu, and Zn in the
641 Azores triple junction hydrothermal vent fields food web. *Chemosphere* **2006**, *65*, 2260-2267.
- 642 85. Kwon, S. Y.; Blum, J. D.; Chen, C. Y.; Meattay, D. E.; Mason, R. P., Mercury isotope study of sources and exposure
643 pathways of methylmercury in estuarine food webs in the Northeastern U.S. *Environ. Sci. Technol.* **2014**, *48*, 10089-10097.

- 644 86. Masbou, J.; Sonke, J. E.; Amouroux, D.; Guillou, G.; Becker, P. R.; Point, D., Hg-Stable Isotope Variations in Marine Top
645 Predators of the Western Arctic Ocean. *ACS Earth Space Chem.* **2018**, *2*, 479-490.
- 646 87. Li, M. L.; Kwon, S. Y.; Poulin, B. A.; Tsui, M. T.; Motta, L. C.; Cho, M., Internal Dynamics and Metabolism of Mercury in
647 Biota: A Review of Insights from Mercury Stable Isotopes. *Environ. Sci. Technol.* **2022**, *56*, 9182 – 9195.
- 648 88. Renedo, M.; Bustamante, P.; Cherel, Y.; Pedrero, Z.; Tessier, E.; Amouroux, D., A "seabird-eye" on mercury stable isotopes
649 and cycling in the Southern Ocean. *Sci. Total Environ.* **2020**, *742*, 140499.
- 650 89. Meng, M.; Sun, R.; Liu, H.; Yu, B.; Yin, Y.; Hu, L.; Chen, J.; Shi, J.; Jiang, G., Mercury isotope variations within the marine
651 food web of Chinese Bohai Sea: Implications for mercury sources and biogeochemical cycling. *J. Hazard. Mater.* **2020**, *384*,
652 121379.
- 653 90. Kwon, S. Y.; Blum, J. D.; Chen, C. Y.; Meatey, D. E.; Mason, R. P., Mercury Isotope Study of Sources and Exposure
654 Pathways of Methylmercury in Estuarine Food Webs in the Northeastern U.S. *Environ. Sci. Technol.* **2014**, *48*, (17), 10089-10097.
- 655 91. Tsui, M. T. K.; Blum, J. D.; Kwon, S. Y.; Finlay, J. C.; Balogh, S. J.; Nollet, Y. H., Sources and Transfers of Methylmercury
656 in Adjacent River and Forest Food Webs. *Environ. Sci. Technol.* **2012**, *46*, (20), 10957-10964.
- 657 92. Jiskra, M.; Heimbürger-Boavida, L.-E.; Desgranges, M.-M.; Petrova, M. V.; Dufour, A.; Ferreira-Araujo, B.; Masbou, J.;
658 Chmeleff, J.; Thyssen, M.; Point, D.; Sonke, J. E., Mercury stable isotopes constrain atmospheric sources to the ocean. *Nature*
659 **2021**, *597*, (7878), 678-682.
- 660 93. Foucher, D.; Hintelmann, H.; Al, T. A.; MacQuarrie, K. T., Mercury isotope fractionation in waters and sediments of the
661 Murray Brook mine watershed (New Brunswick, Canada): Tracing mercury contamination and transformation. *Chemical Geology*
662 **2013**, *336*, 87-95.
- 663 94. Smith, R. S.; Wiederhold, J. G.; Kretzschmar, R., Mercury Isotope Fractionation during Precipitation of Metacinnabar
664 (β -HgS) and Montroydite (HgO). *Environ. Sci. Technol.* **2015**, *49*, (7), 4325-4334.
- 665 95. Mil-Homens, M.; Blum, J.; Canário, J.; Caetano, M.; Costa, A. M.; Lebreiro, S. M.; Trancoso, M.; Richter, T.; de Stigter, H.;
666 Johnson, M.; Branco, V.; Cesário, R.; Mouro, F.; Mateus, M.; Boer, W.; Melo, Z., Tracing anthropogenic Hg and Pb input using
667 stable Hg and Pb isotope ratios in sediments of the central Portuguese Margin. *Chem. Geol.* **2013**, *336*, 62-71.
- 668 96. Yin, R.; Feng, X.; Chen, B.; Zhang, J.; Wang, W.; Li, X., Identifying the sources and processes of mercury in subtropical
669 estuarine and ocean sediments using Hg isotopic composition. *Environ. Sci. Technol.* **2015**, *49*, 1347-55.
- 670 97. Araujo, B. F.; Hintelmann, H.; Dimock, B.; Almeida, M. G.; Rezende, C. E., Concentrations and isotope ratios of mercury in
671 sediments from shelf and continental slope at Campos Basin near Rio de Janeiro, Brazil. *Chemosphere* **2017**, *178*, 42-50.
- 672 98. Ogrinc, N.; Hintelmann, H.; Kotnik, J.; Horvat, M.; Pirrone, N., Sources of mercury in deep-sea sediments of the
673 Mediterranean Sea as revealed by mercury stable isotopes. *Sci. Rep.* **2019**, *9*, 1-9.
- 674